Articles
doi.org/10.1002/batt.202000023

Chemistry Europe
European Chemical Societies Publishing

Special Collection

Thickness-Dependent Impedance of Composite Battery Electrodes Containing Ionic Liquid-Based Electrolytes

Marvin Cronau[+],[a] Moritz Kroll[+],[a] Marvin Szabo,[a] Fabian Sälzer,[a] and Bernhard Roling*[a]

Lithium-ion battery models often neglect the salt concentration polarization inside the electrolyte-filled pores of the composite electrodes. However, this concentration polarization causes a significant impedance, in particular in the case of electrolytes with low Li^+ transference numbers. Here, we analyze in detail measured and calculated impedance spectra of composite electrodes containing a solvate ionic liquid-based electrolyte and an ionic liquid-based electrolyte, respectively, in comparison to a conventional carbonate-based electrolyte. For calculating spectra, we use a recently published model by Huang and Zhang. We find that the impedance at 10^{-4} Hz, which is relevant for battery cycling rates around 1 C to 2 C, increases in the order carbonate-based electrolyte < ionic liquid-based electrolyte < solvate ionic liquid-based electrolytes, but exhibits a remarkably weak thickness dependence, when the electrode thickness exceeds 50–100 μm. This suggests that electrodes considerably thicker than the conventional 80 μm can be used in batteries without significantly deteriorating battery power.

1. Introduction

In state-of-the-art lithium-ion batteries (LIBs), the liquid electrolyte is based on volatile organic carbonates. Due to the high vapor pressure, the electrolyte is flammable, leading to serious safety concerns.[1,2] Consequently, a lot of current research is devoted to the study of alternative electrolytes with low vapor pressure and high thermal and electrochemical stability. These are e.g. solvate ionic liquids,[3–6] solvent-in-salt electrolytes,[7–10] and ionic liquid/Li salt mixtures.[11–13] The Li^+ ion transport in these alternative electrolytes is, however, slower than in the carbonate-based electrolytes. Therefore, it is important to carry out comprehensive studies of the ion transport properties of these electrolytes and to use the results for assessing the influence of the electrolyte on the battery impedance. Here, the impedance of the composite electrodes is particularly relevant, since the electrodes are considerably thicker (typically around 80 μm) than the electrolyte-filled separator (typically around 20 μm). During stationary battery cycling, a salt concentration gradient is formed inside the electrolyte-filled pores of the composite electrode leading to anion blocking and stationary Li^+ ion transport. The impedance due to this salt concentration polarization increases with decreasing ionic conductivity and decreasing Li^+ transference number of the electrolyte.[14] Consequently, the salt concentration polarization impedance in the case of solvate ionic liquid-based electrolytes, solvent-in-salt electrolytes, and ionic liquid-based electrolytes is expected to be higher than in the case of carbonate-based electrolytes. However, this concentration polarization impedance is often not explicitly taken into account in battery impedance models, see e.g. Ref. [15], which may be acceptable for carbonate-based electrolytes, but is problematic for alternative electrolytes with slower Li^+ ion transport. Recently, Huang and Zhang published an analytical model for the impedance of composite electrodes explicitly taking into account the salt concentration polarization inside the electrolyte-filled pores of the composite electrodes.[16]

In this paper, we analyze in detail measured and calculated impedance spectra of composite cathodes containing three different classes of electrolytes: (i) A solvate ionic liquid consisting of a 50:50 molar ratio of tetraglyme (G4) with LiTFSI; (ii) a conventional carbonate-based electrolyte, 1 M $LiPF_6$ in EC/EMC 50:50; (iii) a mixture of the ionic liquid *N*-methyl-*N*-propylpyrrolidinium bis(fluorosulfonyl)imide ($Pyrr_{13}FSI$) with the Li salt LiFSI in a molar ratio of 60:40. This molar ratio was chosen, since this mixture exhibits the best ion transport properties.[17] The chemical structures of these electrolytes is illustrated in Figure 1. For calculating the impedance spectra, we use the model by Huang et al..[16] We compare experimental and model spectra of composite electrodes with variable thickness, but constant porosity, and we analyze in detail the different contributions to the electrode impedance in dependence of the thickness. We note that the impedance spectra of composite electrodes up to 50 μm thickness containing a standard carbonate-based electrolyte have been analyzed recently by Gruet et al..[18] Here, we consider also thicker electrodes up to about 150–200 μm, and we pay special attention to the electrode impedance at a frequency of 10^{-4} Hz, which is relevant for battery cycling with rates around 1 C to 2 C. We find that this impedance depends on the type of electrolyte, but exhibits a remarkably weak thickness depend-

[a] M. Cronau,[+] M. Kroll,[+] M. Szabo, F. Sälzer, Prof. Dr. B. Roling
Department of Chemistry, University of Marburg
Hans-Meerwein-Str. 4, D-35032 Marburg, Germany
E-mail: roling@staff.uni-marburg.de

[+] These authors contributed equally to this work.

Supporting information for this article is available on the WWW under https://doi.org/10.1002/batt.202000023

Special Collection An invited contribution to a Special Collection on Electrolytes for Electrochemical Energy Storage

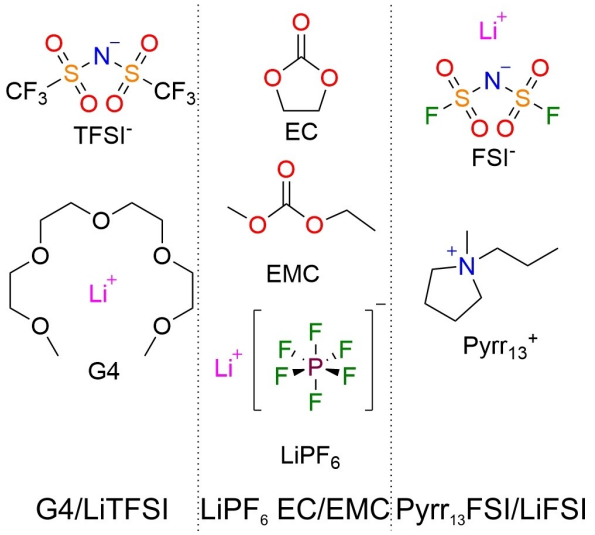

Figure 1. Chemical structures of the studied solvate ionic liquid-based electrolyte, carbonate-based electrolyte, and ionic liquid-based electrolyte.

ence, when the electrode thickness exceeds 50–100 µm. To our knowledge, this weak thickness dependence has not yet been reported and discussed in the literature.

Experimental Section

Preparation of electrolytes

The conventional carbonate-based electrolyte was purchased from Sigma Aldrich (Steinheim, Germany). The solvate ionic liquids were prepared by dissolving LiTFSI (Sigma Aldrich, Steinheim, Germany, 99.95%) in tetraglyme (Sigma Aldrich, Steinheim, Germany, >99%) at room temperature. The ionic liquid/lithium salt mixtures were prepared by dissolving LiFSI (TCI GmbH, Zwijndrecht, Belgium, 98.00%) in $Pyrr_{13}FSI$ (Fluorochem Ltd., Derbyshire, United Kingdom, battery grade) at room temperature.

Electrode preparation

$LiCoO_2$ (LCO) composite electrodes with variable thickness were prepared from an *N*-Methyl-2-pyrrolidone-based (NMP 99.5%, Alfa Aesar, Thermo Fischer GmbH, Kandel, Germany) slurry of 90 wt% LCO (97%, Alfa Aesar), 5 wt% C-NERGY SUPER C 65 carbon black (Timcal, Bodio, Switzerland), and 5 wt% polyvinylidene fluoride (PVDF, Solvay GmbH, Hannover). To this end, the binder was dissolved in NMP at 40 °C, and LCO particles and carbon black were added gradually. The slurry was mixed by means of a T 25 disperser (IKA, Staufen, Germany) and then casted onto an aluminum foil, whereby the thickness of the resulting films was adjusted by means of a ZAA 2300 automatic film applicator (Zehntner, Sissach, Switzerland). The foils were dried for 24 hours at 80 °C under air atmosphere and then transferred into an argon-filled glovebox (UniLab, MBraun, Germany; $x_{H2O} < 1$ ppm, $x_{O2} < 1$ ppm). The porosity of the composite electrodes was determined from the mass, the area and the thickness of the electrodes, taking into account the densities of the electrode components. In order to adjust the porosity of the electrodes to a value of 35%, the films were compacted by using a hot rolling press (MSK-HRP-01, MTI Corporation, Richmond, USA). Discs with a diameter of 12 mm were then cut out of the resulting films. The thickness and weight of each disc electrode including the current collector was determined to calculate the porosity. To this end, a micrometer screw (IP65, Mitutoyo Deutschland GmbH, Neuss) with an error of ±1 µm was used. To determine the weight, we used an analytical balance inside an argon-filled glovebox. To calculate the porosity of each electrode, the mean weight and height of the aluminum current collector was subtracted. To this end, the weight and thickness of 50 aluminum discs with the same diameter were measured. This led to a mean weight of 9.3 ± 0.1 mg and a mean thickness of 32.8 ± 1.3 µm.

Battery cycling

Battery cycling was performed in a TSC battery cell (rhd instruments, Darmstadt, Germany), using a Multi Autolab/M101 (Metrohm Autolab BV, Utrecht, Netherlands). The cells were assembled in an argon-filled glovebox (UniLab, MBraun, Germany; $x_{H2O} <$ 1 ppm, $x_{O2} < 1$ ppm). The battery cycling was carried out in a three-electrode setup with the LCO composite electrode as working electrode and Li metal foil (Albemarle, Germany) as counter and quasi-reference electrode. Working and counter electrodes were separated by 8 layers of Whatman GF/A glass microfiber filters (GE Healthcare, Buckinghamshire, United Kingdom). The separators were soaked with 240 µl of the respective electrolyte. The cells were equilibrated over night at room temperature before starting the cycling.

Electrochemical impedance spectroscopy

The electrochemical impedance measurements were carried out by means of a Multi Autolab/M101 equipped with a FRA32M impedance modul (Metrohm Autolab BV, Utrecht, Netherlands) in a three-electrode setup. The spectra were taken at 50% of the maximum discharge capacity achieved with the respective electrolyte. The frequency range extended from 1 MHz to 10^{-4} Hz with an applied AC voltage amplitude of 10 mV at the open-circuit potential of the respective charge state. Impedance spectra were analyzed using the software RelaxIS 3 (rhd instruments, Darmstadt, Germany).

Calculation of impedance spectra

The complex impedance of the composite LCO cathodes was calculated using the model published by Huang and Zhang[16] To this end, the model was implemented as a Visual C# plugin to the RelaxIS Circuit Simulator (rhd instruments, Darmstadt, Germany). The input parameters are listed in Table 1. The mean radius of the active material particles R_{ap} was determined from an SEM image (Figure S1). The surface of the active material particles was then estimated by assuming spherical particles with the mean radius. The ion transport tortuosity τ_{ion} was determined from EIS measurements under ion-blocking conditions at the electrolyte/LCO particle interface based on the conventional transmission line model (see Supporting Information for more details).[19,20] In order to assess the dependence of the electrode potential on the Li concentration in the active material particles, the charge/discharge potentials of a thin electrode with high porosity (resulting in low overpotentials) was plotted vs. the Li concentration (Figure S3). At the end of the charging process, the stoichiometry of LCO is $Li_{0.5}CoO_2$. The derivative dU/dc_s was determined from the slope at 50% state of charge ($Li_{0.75}CoO_2$). The electronic resistance was assumed to be negligible due to the usage of a conductive carbon additive.

Table 1. Parameters for the calculation of impedance spectra using the model of Huang and Zhang[16] for LCO composite cathodes containing G4/LiTFSI 50:50 or 1 M $LiPF_6$ in a carbonate mixture as electrolyte.

Parameter	Physical meaning	Value G4/LiTFSI 50:50	Value 1 M $LiPF_6$ in carbonates
σ_{ion}	Ionic conductivity	0.152 S m^{-1}[21]	1 S m^{-1}[22]
D_{salt}	Salt diffusion coefficient	$6.96\cdot10^{-12}$ m^2 s^{-1}[22]	$3\cdot10^{-10}$ m^2 s^{-1}[22]
$\frac{d\ln(a_{+-})}{d\ln(c_{salt})}$	Thermodynamic factor	30[23]	2[24]
t_+^{μ}	Mobility-based Li^+ transference number of the electrolyte	0.45[17]	0.35[22]
c_{salt}	Salt concentration	2640 mol m^{-3}[23]	1000 mol m^{-3}
j_0	Exchange current density for cathode active material particles	1 A m^{-2}	0.124 A m^{-2}
T	Temperature	303.15 K	
m_{ap}	Active material weight per electrode thickness	0.3115 kg m^{-1}	
R_{ap}	Radius of the active material particles	$1.7\cdot10^{-6}$ m	
ρ_{ap}	Active material mass density	5060 kg m^{-3}	
ε_e	Electrode porosity	0.35	
τ_{ion}	Ionic tortuosity	2.7	
dU/dc_s	Dependence of electrode potential on Li^+ concentration in the active material particles	$-6.68\cdot10^{-6}$ V m^3 mol^{-1}	
C_{DL}	double layer capacitance	$5\cdot10^{-2}$ F m^{-2}	
D_s	Li chemical diffusion coefficient in active material particle	$1\cdot10^{-15}$ m^2 s^{-1}[25]	

2. Results and Discussion

In Figure 2, we compare the galvanostatic charge/discharge curves of LCO composite cathodes with a thickness of 66–67 µm containing one of the three electrolytes. The discharge capacity of commercial LCO is typically in the range of 160–170 mAh g^{-1}.[26] In the case of the carbonate-based electrolyte 1 M $LiPF_6$ in EC/EMC 50:50, this typical discharge capacity is achieved. In contrast, with the two alternative electrolytes, lower discharge capacities are observed, namely about 30 mAh g^{-1} in the case of the G4/LiTFSI 50:50 and about 85 mAh g^{-1} in the case of $Pyrr_{13}FSI$/LiFSI 60:40. In order to estimate the area-specific effective resistances during galvanostatic cycling, the charge and discharge overpotential at SOC50 was taken, since the impedance spectra were also taken at this SOC. The difference between the charge and discharge potential at SOC50 was identified with the sum of the charge and the discharge overpotential. By taking into account the current density, the following area-specific effective resistances were estimated: (i) about 130 Ω cm^2 in the case of G4/LiTFSI 50:50; (ii) about 30 Ω cm^2 in the case of 1 M $LiPF_6$ in EC/EMC 50:50; (iii) about 95 Ω cm^2 in the case of $Pyrr_{13}FSI$/LiFSI 60:40.

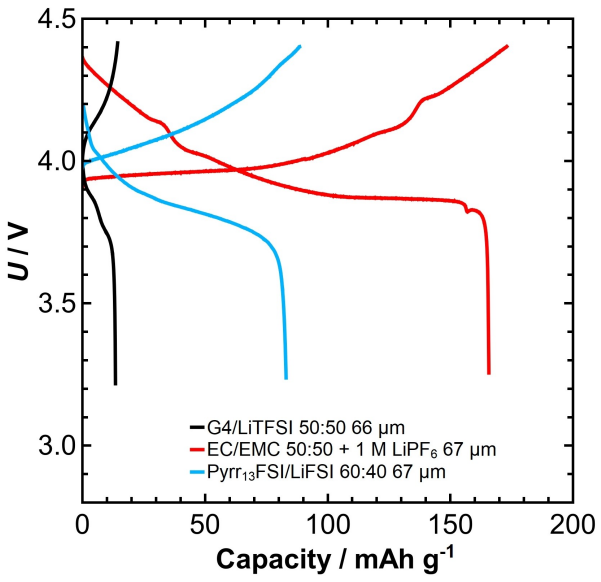

Figure 2. First galvanostatic cycle of LCO composite electrodes with a thickness of 66–67 µm containing different electrolytes. The electrodes were cycled with a C rate of 0.26 C (44 mA g^{-1}).

In Figure 3a–c we show measured impedance spectra taken for composite electrodes of variable thickness containing one of the three electrolytes. The insets show zooms into the high-frequency regime of the spectra. We note that all spectra exhibit a high-frequency resistance, which is caused by the electrolyte-filled separator between the composite LCO working electrode and the quasi-reference electrode. In Figure 3, this high-frequency resistance is subtracted in order to show exclusively the impedance of the LCO composite electrode. The high-frequency impedance of this composite electrode down to about 1 Hz is characterized by a transmission-line-type impedance caused by the ion migration resistance of the composite electrodes, R_{ion}, and the charge transfer resistance R_{ct} for Li^+ ions at the electrolyte/active material interface.[27] At frequencies below 1 Hz, a Warburg-type impedance is detected. In all spectra, the impedance measured at the lowest frequency of 10^{-4} Hz is indicated, since this impedance is relevant for typical battery cycling rates around 1 C–2 C. This cycling rate implies a cycling time scale of $\tau = 1$ hour $= 3600$ s, corresponding to a frequency of $1/(2\pi\tau) \approx 4\cdot 10^{-5}$Hz. Since our lowest measurement frequency of 10^{-4} Hz is close to $1/(2\pi\tau)$, the impedance at this frequency should be similar to the effective resistance of the composite electrode during 1 C–2 C cycling. For the electrode thicknesses in the range of 66–67 µm, we obtain the following order of $Z'(10^{-4}$ Hz) values: G4/LiTFFSI 50:50 > $Pyrr_{13}FSI$/LiFSI 60:40 > 1 M $LiPF_6$ in EC/EMC 50:50. This is the same order as obtained for the effective resistances from the galvanostatic charge/discharge curves shown in Figure 2.

In Figure 4a and b we show in comparison calculated impedance spectra for composite electrodes containing the two electrolytes G4/LiTFSI 50:50 and 1 M $LiPF_6$ in a carbonate mixture. The very-low-frequency spikes due to the chemical capacitance of the active material particles are shown in

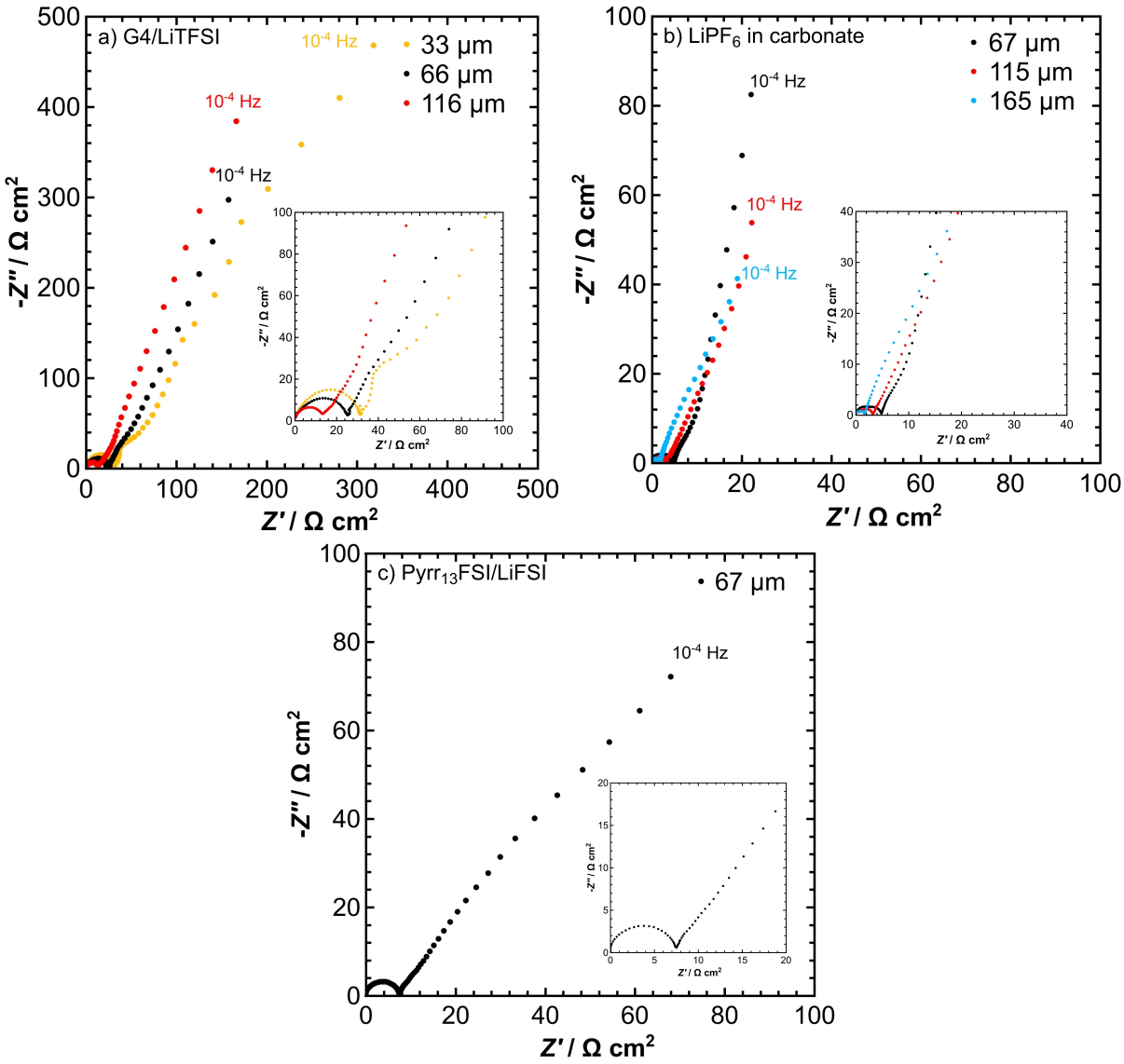

Figure 3. Impedance spectra (frequency range: 10^3 Hz to 10^{-4} Hz) of LCO composite electrodes with varying thicknesses. a) G4/LiTFSI 50:50, thicknesses between 33 µm and 116 µm. b) 1 M $LiPF_6$ in EC/EMC 50:50, thicknesses between 67 µm and 165 µm. c) $Pyrr_{13}FSI$/LiFSI 60:40, thickness of 67 µm. The insets show zooms into the high-frequency range.

Figure S4. The spectra were calculated by means of the impedance model by Huang and Zhang,[16] which is only applicable to electrolytes containing a single type of cations and a single type of anions. Consequently, it cannot be used for calculating impedance spectra of the ionic liquid-based electrolyte $Pyrr_{13}FSI$/LiFSI containing three types of ions. The high-frequency semicircle is due to ion migration resistance and the charge transfer resistance, while the low-frequency semicircle is caused by the salt concentration polarization impedance (see Figure S5). The model spectra are similar to the measured spectra, not only with regard to the spectral shape, which will be discussed later in more detail, but also regarding the dependence of the impedance on the electrode thickness. In the case of G4/LiTFSI 50:50, we observe a decrease of $Z'(10^{-4}\ \mathrm{Hz})$ with increasing thickness of the electrode, see Figure 3a and Figure 4a. In the case of 1 M $LiPF_6$ in EC/EMC/PC, the real part of the impedance at 10^{-4} Hz, $Z'(10^{-4}\ \mathrm{Hz})$, depends only weakly on the thickness of the composite electrode, see Figure 4b. This weak dependence is also observed in the experimental spectra in Figure 3b.

In Figure 5, we consider the thickness dependence of the calculated electrode resistances in more detail. We compare the electrode resistance in the limit of zero frequency $R_{zf} = Z'(\nu \to 0)$ with the real part and the modulus of the impedance at 10^{-4} Hz, $Z'(10^{-4}\ \mathrm{Hz})$ and $|Z|(10^{-4}\ \mathrm{Hz})$. At low electrode thicknesses, R_{zf} decreases with increasing thickness. With further increasing thickness R_{zf} goes through a minimum and then increases. In contrast, $Z'(10^{-4}\ \mathrm{Hz})$ and $|Z|(10^{-4}\ \mathrm{Hz})$ decrease essentially with increasing thickness, but beyond 100 µm, $Z'(10^{-4}\ \mathrm{Hz})$ and $|Z|(10^{-4}\ \mathrm{Hz})$ exhibit only a very weak thickness dependence.

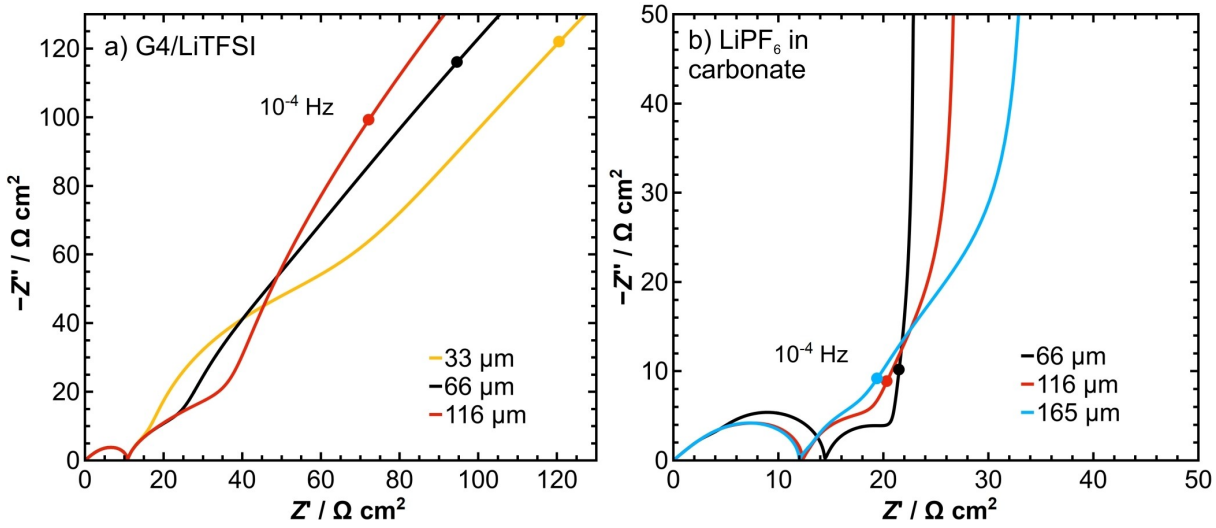

Figure 4. Calculated impedance spectra of a LCO composite cathode with a) G4/LiTFSI 50:50 and b) $LiPF_6$ in carbonate as electrolyte.

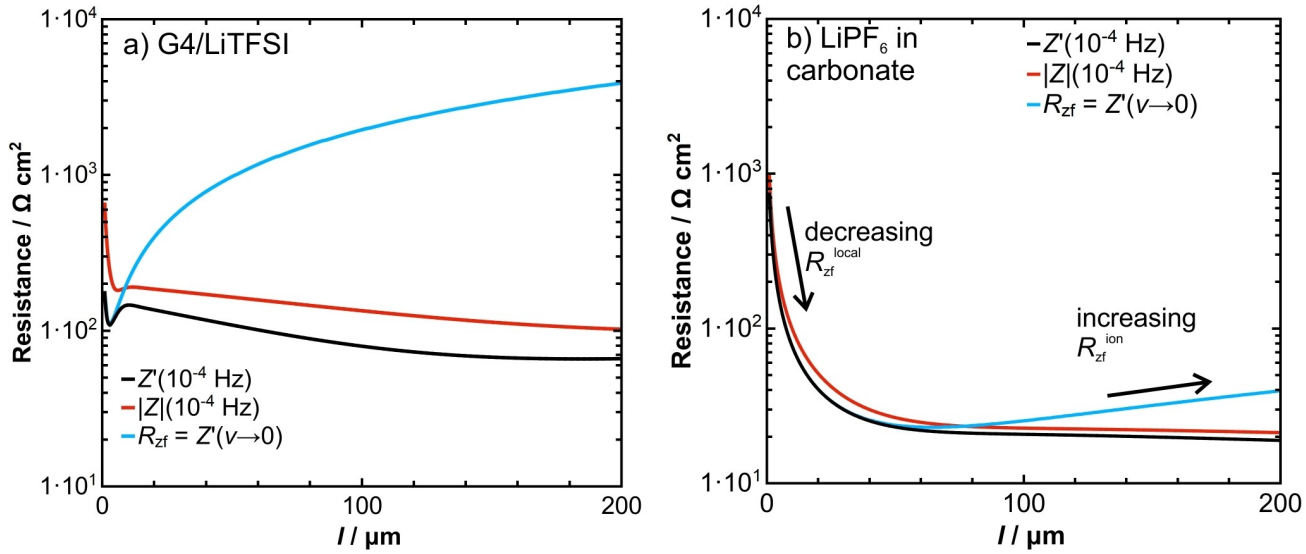

Figure 5. Dependence of the zero-frequency electrode resistance R_{zf} and of the real part and the modulus of the impedance at 10^{-4} Hz, Z' (10^{-4} Hz), and $|Z|(10^{-4}$ Hz) on electrode thickness when using a) G4/LiTFSI 50:50 and b) $LiPF_6$ in carbonate as electrolyte.

In the following, we discuss the origin of these thickness dependences. In a recent paper, we showed that low-frequency impedance spectra of a porous electrode in the framework of the Huang and Zhang model can be approximated by a modified transmission-line model expression [Eq. (1)]:[17]

$$Z_{pe}^{lf-TLM} = \sqrt{\frac{Z_{loc}}{a_v \cdot \sigma_{Li^+}^{ABC,eff}}} \cdot \coth\left(\sqrt{\frac{a_v \cdot l_p^2}{\sigma_{Li^+}^{ABC,eff} \cdot Z_{loc}}}\right) \quad (1)$$

Here, $\sigma_{Li^+}^{ABC,\,eff} = t_{Li^+}^{ABC} \cdot \sigma_{ion}^{eff}$ is the effective ionic conductivity of the composite electrode under anion-blocking conditions. $\sigma_{ion}^{eff} = \frac{\sigma_{ion}\,\varepsilon_e}{\tau_{ion}}$ is the effective ionic conductivity of the composite electrode without salt concentration polarization, and $t_{Li^+}^{ABC}$ is the Li^+ ion transference number under anion-blocking conditions. The pore length is denoted by $l_p = l \cdot \tau_{ion}$, and $a_v = \frac{3(1-\varepsilon_e)}{R_{ap}}$ corresponds to the surface of the active material particles per unit volume of the electrode. The local impedance Z_{loc} is given by:

$$Z_{loc} = \left(\left(R_{CT} + \frac{dU}{dc_s} Y_s\right)^{-1} + i\omega C_{DL}\right)^{-1} \quad (2)$$

with

$$Y_s = \frac{R_{ap}}{FD_s} \cdot \frac{\tanh(\Omega_s)}{\tanh(\Omega_s) - \Omega_s} \quad (3)$$

and

$$\Omega_s = \sqrt{\frac{i\omega R_{ap}^2}{D_s}} \tag{4}$$

$R_{CT} = \frac{RT}{Fj_0}$ is the area-specific charge transfer resistance at the electrode/active material particle interface. The other parameters are explained in Table 1. Eq. (1) describes the impedance under the assumption that the salt concentration polarization in the electrolyte-filled pores of the electrode is complete (complete anion blocking), but the Li^+ chemical diffusion inside the active material particles still takes place. A zero-frequency Taylor expansion of Eq. (1) results in the following expression for the real part of the electrode impedance in the zero-frequency limit, R_{zf}:

$$R_{zf} = \underbrace{\frac{l_p}{3\sigma_{ion}^{ABC,eff}}}_{R_{zf}^{ion}} + \underbrace{\frac{R_{CT}}{a_v l_p} - \frac{R_{ap}}{5FD_s a_v l_p} \cdot \frac{dU}{dc_s}}_{R_{zf}^{local}} \tag{5}$$

The first term on the right-hand side of Eq. (5) describes the Li^+ ion transport limitations due to concentration polarization and anion-blocking and is in the following denoted by R_{zf}^{ion}. The second term accounts for the charge transfer at the electrolyte/LCO interface and the third term for the resistance due to Li chemical diffusion into the active material particles. The second and the third term arise from the local impedance given in Eqs. (2)–(4). Therefore, the sum of the second and of the third term is denoted in the following by R_{zf}^{local}. While the ion transport resistance R_{zf}^{ion} increases with the electrode thickness l, the local resistance R_{zf}^{local} decreases with l. For thin electrodes, R_{zf}^{local} dominates and leads to a decrease of R_{zf} with increasing l. At thick electrodes, R_{zf}^{ion} dominates and leads to an increase of R_{zf} with increasing l, see Figure 5.

In order to elucidate the origin of the weak thickness dependence of $Z'(10^{-4}\ \text{Hz})$ and $|Z|(10^{-4}\ \text{Hz})$, we approximate the impedance by a more general transmission-line type equation:

$$Z_{pe}^{\text{general TLM}} = \sqrt{\frac{Z_{ion} \cdot Z_{loc}}{l_p \cdot a_v}} \cdot \coth\left(\sqrt{\frac{Z_{ion} \cdot l_p \cdot a_v}{Z_{loc}}}\right) \tag{6}$$

with

$$Z_{ion} = \frac{l_p}{\sigma_{ion}^{eff}} + \left(\frac{l_p}{\sigma_{ion}^{ABC,eff}} - \frac{l_p}{\sigma_{ion}^{eff}}\right) \frac{\tanh(\Omega_{ion})}{\Omega_{ion}} \tag{7}$$

and

$$\Omega_{ion} = \sqrt{\frac{i\omega {l_p}^2}{D_{salt}}} \tag{8}$$

Eq. (6) takes into account the frequency dependence of Z_{ion}, as described by Eqs. (7) and (8), while Eq. (1) contains only the zero-frequency limit of Z_{ion}. These equations are based on a generalized transmission line model (TLM). TLMs are widely used in the literature to describe the response of porous electrodes.[28] In Ref. [28], the TLM with open-open condition and with $Z_C = 0$ leads to Eq. (6). Eq. (7) is derived from the equations for the ion transport impedance between planar electrodes under anion-blocking conditions,[21] and is only modified for porous electrodes by replacing the ionic conductivities by effective ionic conductivities according to the porosity and tortuosity of the electrode.

Two limiting cases of Eq. (6) can be considered: (i) If $Z_{ion} \gg Z_{loc}/(l_p \cdot)$, the coth function becomes unity and the impedance is given by $Z_{pe}^{\text{general TLM}} = \sqrt{\frac{Z_{ion} \cdot Z_{loc}}{l_p \cdot a_v}}$. This impedance is independent of electrode thickness. (ii) If $Z_{loc}/(l_p \cdot a_v) \gg Z_{ion}$, the coth(x) function can be Taylor expanded into $1/x + x/3$. This results in $Z_{pe}^{\text{general TLM}} = Z_{loc}/(l_p \cdot a_v) + Z_{ion}/3$. In this case, the impedance does depend on thickness. Since $Z_{loc}/(l_p \cdot a_v)$ and Z_{ion} exhibit distinct frequency dependences, the ratio of these two impedances is frequency-dependent.

In Figure 6, we plot the modulus of $Z_{loc}/(l_p \cdot a_v)$ and of Z_{ion} versus the frequency for a composite electrode containing the electrolytes G4/LiTFSI 50:50 and 1 M $LiPF_6$ in a carbonate mixture, respectively. Three different electrode thicknesses, 50 μm, 100 μm, and 150 μm are considered. In the case of the electrolyte G4/LiTFSI 50:50, we find that $Z_{ion} \gg Z_{loc}/(l_p \cdot a_v)$ for all thicknesses and over the entire frequency range, see Figure 6a. Consequently, the impedance can be well approximated by $Z_{pe}^{\text{general TLM}} = \sqrt{\frac{Z_{ion} \cdot Z_{loc}}{l_p \cdot a_v}}$. At a frequency of 10^{-4} Hz, the modulus of Z_{ion} is in the range of $10^3\ \Omega\,cm^2$ and depends only weakly on thickness, while the modulus of $Z_{loc}/(l_p \cdot a_v)$ is in the range of 4–12 $\Omega\,cm^2$ and decreases with increasing thickness. Since in this case, $Z_{pe}^{\text{general TLM}}$ is the geometrical average of Z_{ion} and $Z_{loc}/(l_p \cdot a_v)$, its modulus should be in the range of 100–200 Ωcm^2 and should decrease slightly with increasing thickness. As shown in Figure 5a, $|Z|(10^{-4}\ \text{Hz})$ is indeed in the range of 160 Ωcm^2 and decreases slightly with increasing thickness. Thus, the origin of this slight decrease is the decreasing $Z_{loc}/(l_p \cdot a_v)$ due to an increasing interfacial area between electrolyte and LCO particles. In the case of the electrolyte 1 M $LiPF_6$ in a carbonate mixture, the modulus of $Z_{loc}/(l_p \cdot a_v)$ is in a similar range, see Figure 6b. At 10^{-4} Hz we also have $Z_{ion} > Z_{loc}/(l_p \cdot a_v)$ and consequently the impedance $Z_{pe}^{\text{general TLM}}$ should become virtually independent of thickness at 10^{-4} Hz. As shown in Figure 5b, Z' $(10^{-4}\ \text{Hz})$ and $|Z|(10^{-4}\ \text{Hz})$ for the electrolyte 1 M $LiPF_6$ in a carbonate mixture depend indeed very weakly on thickness, when the thickness exceeds about 50 μm.

Thus we can state that for both electrolytes, the thickness dependence of Z' $(10^{-4}\ \text{Hz})$ and of $|Z|(10^{-4}\ \text{Hz})$ is much weaker than the thickness dependence of the zero-frequency limit R_{zf} given in Eq. (5). This suggests that it should be possible to use battery electrodes considerably thicker than the conventional 80 μm without significantly deteriorating battery power at cycling rates around 1 C–2 C. A prerequisite is, however, that the composite electrode morphology and thus the ion trans-

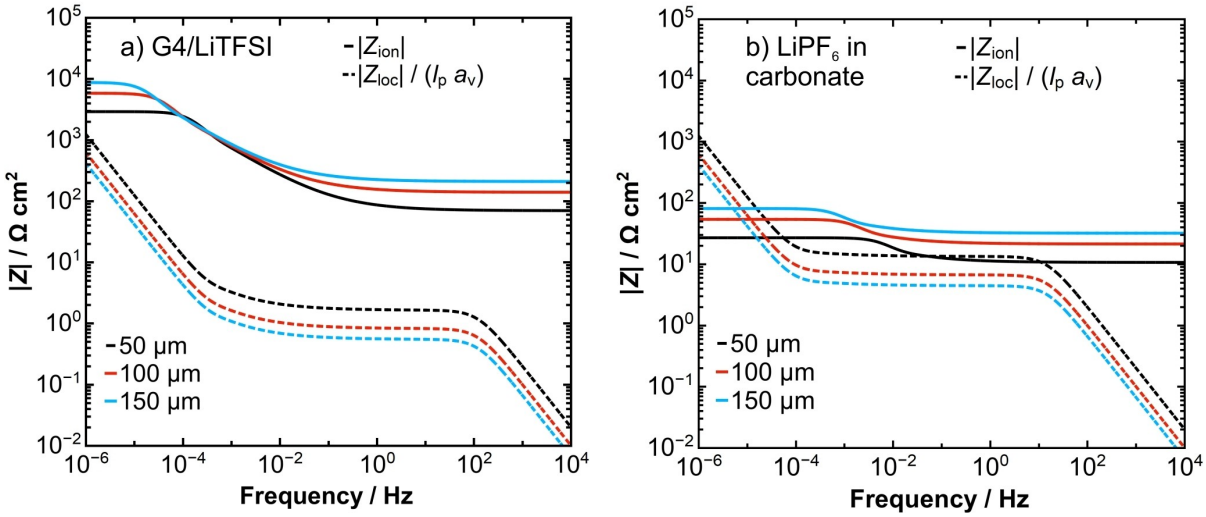

Figure 6. Frequency dependence of the ion transport impedance Z_{ion} and of the local impedance $Z_{loc}/(l_p \cdot a_v)$ for different electrode thicknesses when using a) G4/LiTFSI 50:50 and b) 1 M $LiPF_6$ in carbonate as electrolyte.

port tortuosity can be held constant over the entire thickness range. In this context, it is worth noting that recently Gao et al. reported an increasingly sluggish Li^+ ion transport when increasing the thickness of Ni–Mn–Co oxide (NMC) composite electrodes above 200 µm.[29] Our results suggest that this sluggish Li^+ transport is caused by morphological changes when increasing the electrode thickness and is *not* an intrinsic feature of thick electrodes.

3. Conclusions

We have analyzed experimental and simulated impedance spectra of composite LCO electrodes containing the electrolytes G4/LiTFSI 50:50 and $Pyrr_{13}$FSI/LiFSI 60:40 in comparison to electrodes containing the conventional electrolyte 1 M $LiPF_6$ in EC/EMC 50:50. The results show that the electrode impedance increases in the order 1 M $LiPF_6$ in EC/EMC 50:50 < $Pyrr_{13}$FSI/LiFSI 60:40 < G4/LiTFSI 50:50. This is due to the lower ionic conductivity and lower Li^+ ion transference number of the ionic liquid-based and of the solvate ionic liquid-based electrolytes. We focused in particular on the impedance at 10^{-4} Hz, since this frequency is relevant for battery cycling at 1 C–2 C. Remarkably, the real and modulus of this impedance, Z' (10^{-4} Hz) and $|Z|(10^{-4}$ Hz), depend much more weakly on the electrode thickness than the zero-frequency limit of the electrode impedance, $R_{lf} = Z'(\nu \to 0)$. In the framework of a transmission-line approach, we showed that for thick electrodes $\geq$100 µm and at a frequency of 10^{-4} Hz, the ion transport resistance Z_{ion} becomes larger than the local impedance $Z_{loc}/(l_p \cdot a_v)$ for charge transfer and solid-state diffusion. In this case, the composite electrode impedance is given, to a good approximation, by the geometrical average of Z_{ion} and $Z_{loc}/(l_p \cdot a_v)$ and therefore depends only weakly on thickness. This geometrical impedance averaging results also in an electrode impedance at 10^{-4} Hz when using the alternative electrolytes, which is only a factor of 3–5 higher than for the conventional carbonate-based electrolyte. Thus, battery cycling with the alternative electrolytes should be considerably faster than expected from the zero-frequency limit $R_{zf} = Z'(\nu \to 0)$. Furthermore, the weak thickness dependence of Z' (10^{-4} Hz) and $|Z|(10^{-4}$ Hz) suggests that it should be possible to use battery electrodes considerably thicker than the conventional 80 µm, provided that the morphological features of the electrodes and the resulting ion transport tortuosity can be held constant over the entire thickness range.

Acknowledgements

We thank Albemarle for providing lithium metal foil.

Conflict of Interest

The authors declare no conflict of interest.

Keywords: Li-ion batteries · composite electrodes · ionic liquids · solvate ionic liquids · transference number · electrochemical impedance spectroscopy

[1] J. B. Goodenough, Y. Kim, *Chem. Mater.* **2010**, *22*, 587.
[2] P. G. Balakrishnan, R. Ramesh, T. Prem Kumar, *J. Power Sources* **2006**, *155*, 401.
[3] T. M. Pappenfus, W. A. Henderson, B. B. Owens, K. R. Mann, W. H. Smyrl, *J. Electrochem. Soc.* **2004**, *151*, A209.
[4] K. Ueno, K. Yoshida, M. Tsuchiya, N. Tachikawa, K. Dokko, M. Watanabe, *J. Phys. Chem. B* **2012**, *116*, 11323.
[5] K. Ueno, R. Tatara, S. Tsuziki, S. Saito, H. Doi, K. Yoshida, T. Mandai, M. Matsugami, Y. Umebayashi, K. Dokko, M. Watanabe, *Phys. Chem. Chem. Phys.* **2015**, *17*, 8248.
[6] K. Yoshida, M. Tsuchiya, N. Tachikawa, K. Dokko, M. Watanabe, *J. Phys. Chem. C* **2011**, *115*, 18384.

[7] H. Lundgren, J. Scheers, M. Behm, G. Lindbergh, *J. Electrochem. Soc.* **2015**, *162*, A1334.
[8] Y. Yamada, K. Furukawa, K. Sodeyama, K. Kikuchi, M. Yaegashi, Y. Tateyama, A. Yamada, *J. Am. Chem. Soc.* **2014**, *136*, 5039.
[9] J. Zheng, J. A. Lochala, A. Kwok, Z. D. Deng, J. Xiao, *Adv. Sci.* **2017**, *4*, 1700032.
[10] Y. Hu, H. Li, X. Huang, L. Chen, *Electrochem. Commun.* **2004**, *6*, 28.
[11] A. Balducci, *Top. Curr. Chem. (Z)* **2017**, *375*, 20.
[12] K. Xu, *Chem. Rev.* **2014**, *114*, 11503.
[13] C. Liu, X. Ma, F. Xu, L. Zheng, H. Zheng, H. Zhang, W. Feng, X. Huang, M. Armand, J. Nie, H. Chen, Z. Zhou, *Electrochim. Acta* **2014**, *149*, 370.
[14] M. Doyle, J. Newman, *J. Electrochem. Soc.* **1995**, *142*, 3465.
[15] J. Newman, K. E. Thomas-Alyea, *Electrochemical Systems*, John Wiley & Sons., **2004**.
[16] J. Huang, J. Zhang, *J. Electrochem. Soc.* **2016**, *163*, A1983.
[17] F. Sälzer, L. Pateras Pescara, F. Franke, C. Müller, J. Winkler, M. Schwalm, B. Roling, *Batteries & Supercaps* **2019**, *22*, 587.
[18] D. Gruet, B. Delobel, D. Sicsic, I. T. Lucas, V. Vivier, *Electrochim. Acta* **2019**, *295*, 787.
[19] J. Landesfeind, A. Ehrl, M. Graf, W. A. Wall, H. A. Gasteiger, *J. Electrochem. Soc.* **2016**, *163*, A1254.
[20] M. Kroll, D. Hlushkou, S. Schlabach, A. Höltzel, B. Roling, U. Tallarek, *J. Electrochem. Soc.* **2018**, *165*, A3156.
[21] F. Wohde, M. Balabajew, B. Roling, *J. Electrochem. Soc.* **2016**, *163*, A714.
[22] L. O. Valøen, J. N. Reimers, *J. Electrochem. Soc.* **2005**, *152*, A882.
[23] D. Dong, F. Sälzer, B. Roling, D. Bedrov, *Phys. Chem. Chem. Phys.* **2018**, *20*, 29174.
[24] A. Nyman, M. Behm, G. Lindbergh, *Electrochim. Acta* **2008**, *53*, 6356.
[25] J. Xie, N. Imanishi, T. Matsumura, A. Hirano, Y. Takeda, O. Yamamoto, *Solid State Ionics* **2008**, *179*, 362.
[26] Q. Liu, X. Su, D. Lei, Y. Qin, J. Wen, F. Guo, Y. A. Wu, Y. Rong, R. Kou, X. Xiao, F. Aguesse, J. Bareño, Y. Ren, W. Lu, Y. Li, *Nat. Energy* **2015**, *3*, 936.
[27] N. Ogihara, Y. Itou, T. Sasaki, Y. Takeuchi, *J. Phys. Chem. C* **2015**, *119*, 9, 4612.
[28] Z. Siroma, N. Fujiwara, S.-i. Yamazaki, M. Asahi, T. Nagai, T. Ioroi, *Electrochim. Acta* **2015**, *160*, 313.
[29] H. Gao, Q. Wu, Y. Hu, J. P. Zheng, K. Amine, Z. Chen, *J. Phys. Chem. Lett.* **2018**, *9*, 5100.

Manuscript received: January 31, 2020
Version of record online: March 18, 2020